Nano-imaging of environmental dust in human lung tissue by soft and hard X-ray fluorescence microscopy☆

Alessandra Gianoncelli[a,*], Clara Rizzardi[b], Damien Salomon[c], Vincenzo Canzonieri[d], Lorella Pascolo[e]

[a] Elettra-Sincrotrone Trieste S.C.p.A., Strada Statale SS14, km 163.5, Basovizza 34149, Italy
[b] Department of Medical, Surgical, and Health Sciences, University of Trieste, Italy, Piazzale Europa 1, Trieste 34127, Italy
[c] European Synchrotron Radiation Facility, 71 Avenue des Martyrs, 38000 Grenoble, France
[d] Division of Pathology, CRO Centro di Riferimento Oncologico, National Cancer Institute, IRCCS, Aviano, PN, Italy
[e] Institute for Maternal and Child Health, IRCCS Burlo Garofolo, 34137 Trieste, Italy

ARTICLE INFO

Keywords:
X-ray fluorescence
X-ray microscopy
Nanoimaging
Lung
Anthracosis

ABSTRACT

It is well recognized that a large number of pulmonary diseases are induced by the effects of inhaled particulates. Anthracosis is defined as an asymptomatic, mild form of pneumoconiosis caused by the accumulation of "black carbon" in the lungs due to repeated exposure to air pollution or inhalation of smoke or coal dust particles. Since the human population is progressively exposed to an increasing number and doses of anthropogenic micro and nano particles/compounds, there is a pressing urgency to explore toxicological impact arising from these exposures and the molecular mechanisms driving the body defense or possible related diseases. The toxicity mechanisms are clearly related to chemical composition and physical and surface properties of materials. A combination of synchrotron radiation-based (SR-based) nano X-ray fluorescence (XRF) imaging and soft X-ray microscopy was used to chemically characterize environmental particulates (anthracosis) in lung tissues from urban subjects with the aim of better understanding the complex nature of related lungs' deposits. High-resolution XRF analyses performed at ESRF and Elettra synchrotrons allowed discriminating single particles in the heterogeneous aggregates found in the lung tissue. The small particles have variable composition resulting from the different combinations of Ti with O, K and Si, Al and Si, or Zn and Fe with O. Interestingly, simultaneous absorption and phase contrast images showed the particulate morphology and allowed to predict the presence of very dense nanoparticles or high concentration of heavy elements.

1. Introduction

Lung diseases are among the most common medical conditions in the world [1,2]. Tens of millions of people suffer from them due to infections, genetics predisposition and exposure to smoking or inhalants.

Pneumoconiosis is a group of occupational lung diseases caused by inhaled dust particles and fibres, which causes inflammation of the pulmonary parenchyma leading to fibrosis, affecting the airways or alveoli. Among these, coal workers' pneumoconiosis, also known as black lung disease, is caused by long exposure to coal dust, and commonly affects coal miners and others who work with coal. The initial, milder form of the disease is called anthracosis [3–8], an asymptomatic accumulation of black pigment in the lung tissue and in the related lymph nodes, which can be found in varying degrees among most urban dwellers and in tobacco smokers. Air pollution is unavoidable nowadays and consists of a complex mixture of different components with possible synergic toxicological and carcinogenic effects [3,9–14]. Exposure to mineral and organic particulate, especially in the form of fine particles, may induce genetic damage and has been related to an increased risk of cancer in humans [15].

It is problematic to assess the pathogenicity of poorly soluble materials in the form of dust particles and fibres, since their effects are determined not only by the chemical composition but also by their physical properties and biopersistance. Additionally, inside the tissues dust particles and fibres may undergo complex metabolic transformations and their surface may be modified by removal and deposition of chemical elements, metals, and salts, or by adsorption of macromolecules such as proteins [6,16].

Despite the fact that there are many reports and studies on air

☆ Selected Paper from the Colloquium Spectroscopicum Internationale XL (CSI 2017), Pisa, Italy, 11-16 June 2017.

* Corresponding author.
E-mail address: alessandra.gianoncelli@elettra.eu (A. Gianoncelli).

Accepted 22 May 2018

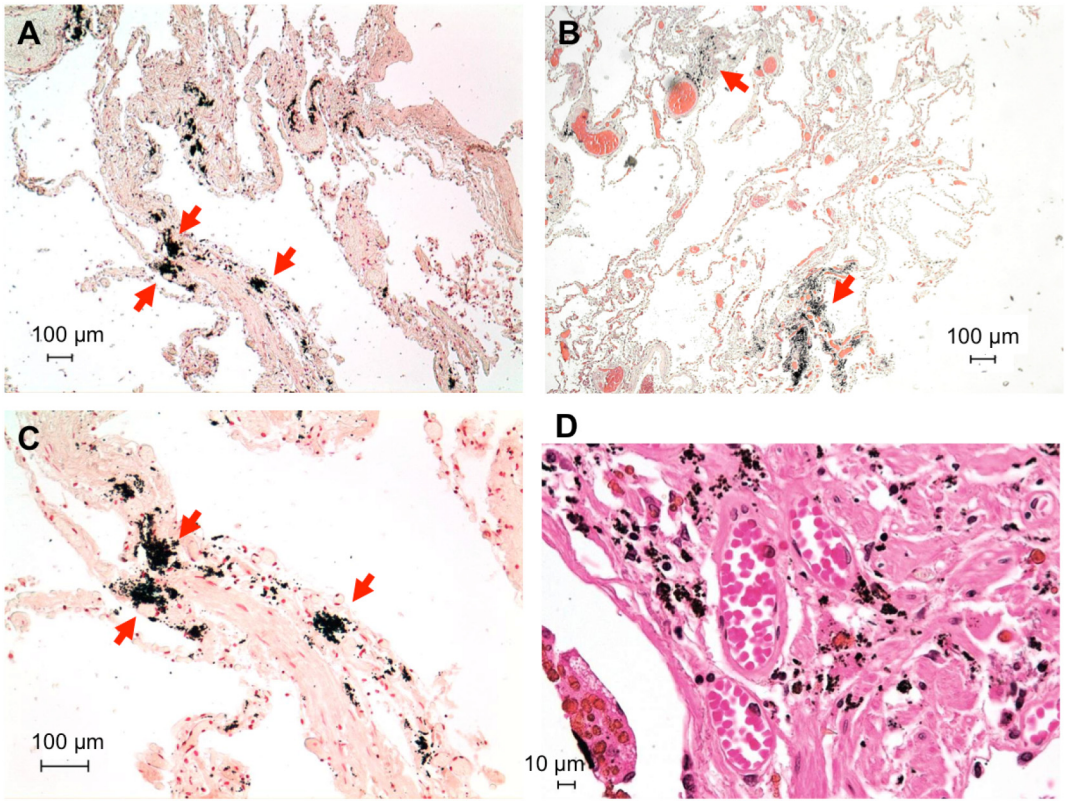

Fig. 1. Photos of hematoxylin and eosin (H&E) stained lung tissues from three different patients (A–C, B and D respectively) and at different magnifications (Panels A and B 10×, Panel C 20× and Panel D 50×) highlighting the presence of black-pigmented deposits in different lung tissue areas: in interlobular septa (A, C), around bronchovascular bundles (B) and in the fibrous tissue (D). Panel C is a higher magnification of Panel A. Scale bar are 100 µm for Panels A, B, C and 10 µm for Panel D.

particulate matter (PM) characterization [17–23] from different part of the world, to our knowledge only a very few sparse examples of lung tissue chemical analyses are reported in literature [6,16,24–28]. There have been a few attempts with SEM and TEM-EDS [29]: although the spatial resolution of these techniques is clearly higher than XRF, the more complicated sample preparation and their lower detection sensitivity limit the information that can be gained from their results [30].

The aim of this work is to apply Synchrotron Radiation X-Ray Fluorescence (SR-µ XRF) spectromicroscopy [31–34] to track the environmental dust particles or fibres inside histological samples of lung tissue and to investigate the chemical nature at nanometer spatial resolution.

In this work, the chemical nature of anthracotic material, found in lung tissues from undefined environmental exposure, was investigated by means of a sequential use of two synchrotron beamlines, ID16B-NA and TwinMic, at two different facilities, ESRF (Grenoble, France) and Elettra Sincrotrone Trieste (Trieste, Italy).

2. Materials and methods

2.1. Patients and sample preparation

Human lung samples were derived from post-mortem examination of three patients which were selected from the archive files of the Unit of Pathology of CRO of Aviano (Italy) [6,16]. The patients had lived in urban centers of the region Friuli Venezia Giulia without known specific professional exposure. Human samples consisted of tissues discarded after forensic autopsy, and were retrieved with the approval of the institution. The identification of anthracosis was performed by light microscopy (DM2500, Leica Microsystems, Germany) on 3–5 µm thick sections from paraffin-embedded samples of non-neoplastic lung tissue both unstained and stained with hematoxylin and eosin (H&E) according to standard protocols. For X-ray imaging and XRF analyses, the unstained 5 µm thick sections were mounted on ultralene foils (4 µm thick) and air-dried, as previously described [16,35,36].

2.2. Synchrotron-based nano X-ray fluorescence analyses

The synchrotron XRF experiments have been carried out at two different synchrotron facilities. In both experiments, the X-ray beam was focused on the sample through suitable X-ray optics and the sample was raster scanned across the beam. For each pixel in the raster scan the X-ray Fluorescence (XRF) was collected by energy dispersive silicon drift detectors (SDD).

The samples were firstly analysed at the ID16B-NA beamline [37] of the European Synchrotron Radiation Facility (ESRF, Grenoble, France) where the pink ($\Delta E/E = 0.01$) 17.54 keV X-ray beam was focused by Kirkpatrick-Baez (KB) mirrors to a spot size of 60 nm × 60 nm on the sample plane (photon flux $4 * 10^{10}$ photons/s). The XRF emitted by the sample were collected by two SGX sensortech SDD arrays, each with an active silicon area of 80 mm^2, using an acquisition time of 100 ms per pixel in the raster scan. A standard reference material from NIST (bovine liver SRM 1577B) was measured for calibration of the X-ray Fluorescence spectra to get semi-quantitative results on some transition metals. Spectra were fitted based on the configuration derived from the measured standard using PyMCA [38] for quantification of the elemental content. The obtained concentrations are expressed in g/g assuming a 1.5 µm thick protein matrix with density 1.2.

Further XRF analyses were carried out on the previously mentioned specimens at the TwinMic beamline [39] (Elettra - Sincrotrone, Trieste, Italy) under a low energy microscopy set-up. TwinMic microscope was operated in scanning transmission mode (STXM) where the beam is focused on the sample through a zone plate diffractive optics (600 µm in diameter with 50 nm outermost zone width) providing sub-micron

spatial resolution. The obtained absorption and phase contrast images outline the morphological features of the sample at sub-micrometer length scales [40], whereas the simultaneous detection of the low energy XRF [41] correlates the elemental distribution to the morphology. For the present experiments we selected a photon energy of 1.95 keV (photon flux $3 * 10^7$ photons/s) to excite and get optimal emission conditions for the elements of major interest, namely Si, Al and Mg and other lighter elements, in particular O and Na, with a spot of 250 nm and a dwell time of 9 s per pixel. The sample was mounted on a x-y stage (with the incoming beam perpendicular to the sample surface) facing a 8 Silicon Drift Detectors placed at 2 cm from the sample [42].

For all XRF maps, the elemental distribution was obtained by processing and deconvolving the XRF spectra with the PyMCA software [38].

3. Results and discussion

Histological examination of the lungs samples of all the patients showed clear features of urban dust exposure. Fig. 1 shows many carbonaceous particles and aggregates in some regions of patients tissue, appearing as collection of black granules. The particles appear concentrated around interlobular septa (A, B), bronchovascular bundles (B) and in the fibrous tissue (D).

From all patients, at least two tissue slices were analysed by XRF and results on dust materials were found comparable. In the studies representative images are presented.

In a previous study [6], we compared the elemental distribution in lung tissues presenting anthracosis and/or asbestos bodies. The analyses were made at 7.3 keV, with sub-micron spatial resolution, highlighting the specificity of the distributions of Ca, P, Fe, Si, Ti and Cr for different pollutants. In the present study we deepened the investigation on anthracotic lung tissues by moving to nanoscale spatial resolution and extending the energy range and therefore increasing the number of detectable chemical elements, thus providing more insights on the particulate chemical nature and its distribution inside the lungs.

Lung tissues samples were first investigated by optical microscopy to identify the regions of interest. As shown in Fig. 1, beside normal lung vessels and cells, several dark/black areas appear in the tissues. Those darkened areas appear to have different sizes and to be composed by multiple macro and nano-aggregates. Although anthracosis is visible also in unstained sections, the staining with hematoxylin and eosin (H&E) (Fig. 1) helps to easily identify the presence of typical lung cells and structures, together with dust particulate.

Afterwards several areas in the unstained slices were scanned at 17.54 keV at ID16B-NA beamline (ESRF, Grenoble, France) with nanometric spatial resolution. From the initial analyses at micron or 500 nm spatial resolution, such as the example in Fig. 2, nanoparticulate dust appears to contain many metals such as Fe, Mn, Cu, Zn, Ti, Cr and Ni, most of them co-localising, although Ti and Cr distribution is peculiar and distinctive, as previously observed by the present authors [6]. Compared to our previous work which was performed at sub-micrometric resolution and at lower energy [6], the current analyses reveal that also Br, Se, Cu, Zn and Sr are frequent and highly concentrated into the anthracotic features; however it is difficult to spatially discriminate their location. Nonetheless with the 60 nm focus of ID16B-NA beamline it appears more clearly that dust is composed of multiple types of nanoparticulate, as depicted in Fig. 3. Based on distinctive appearance or co-localisations, as calculated by Scatter Plot analysis (supporting Fig. S1), it could be speculated that we are detecting at least seven different types of dust nano-deposits: Br-Se based, K-Si based, Fe-Ti based, Cr-based, Ni-based, Fe-based (possible oxides) and Ca-As based, in addition to less defined Zn and/or Cu containing particulate. In addition to Ca-As, scatter plots show a correlation between As and Sr distributions: this is not surprising since Ca and Sr have similar electronic properties. The identification of different types of dust materials is in agreement with studies identifying aerosol particulate as mixtures of numerous chemical species within individual particles [43]. Therefore, it is impossible to discriminate whether the mixtures we find in the lung samples were formed in the airways or before inhalation.

The results are in agreement with previous particulate matter (PM) investigations, in particular with PM2.5 and PM10 chemical compositions. Particulate matter contains a wide range of particle types having different sizes, shape, compositions and optical properties [44]. Many studies from all over the world [19,45,46], some of them performed with XRF technique [47] have shown that air particulate is mainly composed by S, Si, K, Al, Ba, Ca, Ti, Cr, Mn, Fe, Ni, Cu, Zn, and Pb, with Si, Ca and Fe among the dominant chemical elements. While most of these studies were performed directly in air particulate filters, our investigation is performed straight on lung tissue samples without excessive treatment, except for fixation and embedding in paraffin medium.

In Fig. 3 iron is identified in micro and nano-clusters and appears to be highly abundant, in agreement with air particulate composition reported previously [19,45,46]. Iron is often co-localising with trace elements, such as Ti or Br and Se, however, part of the signal is undoubtedly due to endogenous iron [6]. The occurrence of bromine is not surprising since the exposure is very frequent in both urban and rural sites. Bromine is present in sea-salt aerosol particles and in fuel additives [48].

Selenium can be found in the environment both in gaseous and solid form. Selenium solid suspended particles are produced as a result of human activities, such as combustion of coal and other fuels or copper smelting [49] or incineration of waste such as paper products, as with Br [50]. We note that in our samples Se occurrence is highly correlated with Br (Fig. S1), suggesting its origin is incineration of waste.

Fig. 3 shows Ni occurring as nano-formations in the XRF maps, sometimes accompanied by micro-structures. Nickel is an environmental pollutant, which causes mild to severe allergies. In PM this element seems to be present due to anthropogenic pollution such as traffic or industry (oil combustion) [22]. Its detection at the nanometer scale is therefore of importance, allowing for future investigations on the pathological mechanisms associated to its exposure.

It is not easy to completely interpret the occurrence and the hot spots distribution of Cu and Zn since these two elements can be both endogenous and exogenous. When exogenous they are trace elements in industrial products, combustion and fuels emission [51], while as endogenous they are key elements in detoxifying mechanisms and their occurrence could be thus considered as a tissue response to pollutants [52].

By using a reference standard (bovine liver SRM 1577B from NIST) it was possible to quantify in the tissues the concentration of chemical elements whose K emission lines fall in the 6–10 keV energy range: Cr, Mn, Fe, Ni, Cu and Zn. For the other elements the calculation was not reliable. The results in Fig. 3 show that Cr is notably abundant in the nanoparticles reaching an average concentration between 500 and 1000 ppm in the hotspots. Copper is often around 15 ppm with diffuse appearance in the aggregates or in some hot spots reaching up to 100 ppm, while Zinc content in the tissue ranges from 40 to 120 ppm (as endogenous element) whereas in the nanoaggregates is around 700 ppm. This quantification clearly supports the idea that these two elements have also an exogenous origin. Manganese concentration is also notable, reaching up to 0.1% in micrometric areas and 0.2% in some nanoparticulate formations, again suggesting an exogenous origin. Nickel is less abundant, being present with a concentration of around 40 ppm at micrometric scale level and with 100–120 ppm in nanospots. Iron is clearly the most abundant element, ranging from 0.7 to 2% at micrometric scale length but reaching even 5% in nanoclusters.

An intriguing result shown in Fig. 3 is the occurrence of As in nanoscale aggregates, with high co-localisation with Ca and/or Sr in several micro-regions, as also highlighted by the scatter plots in Fig. S1. We note As is a main component of PM in areas with industrial activity

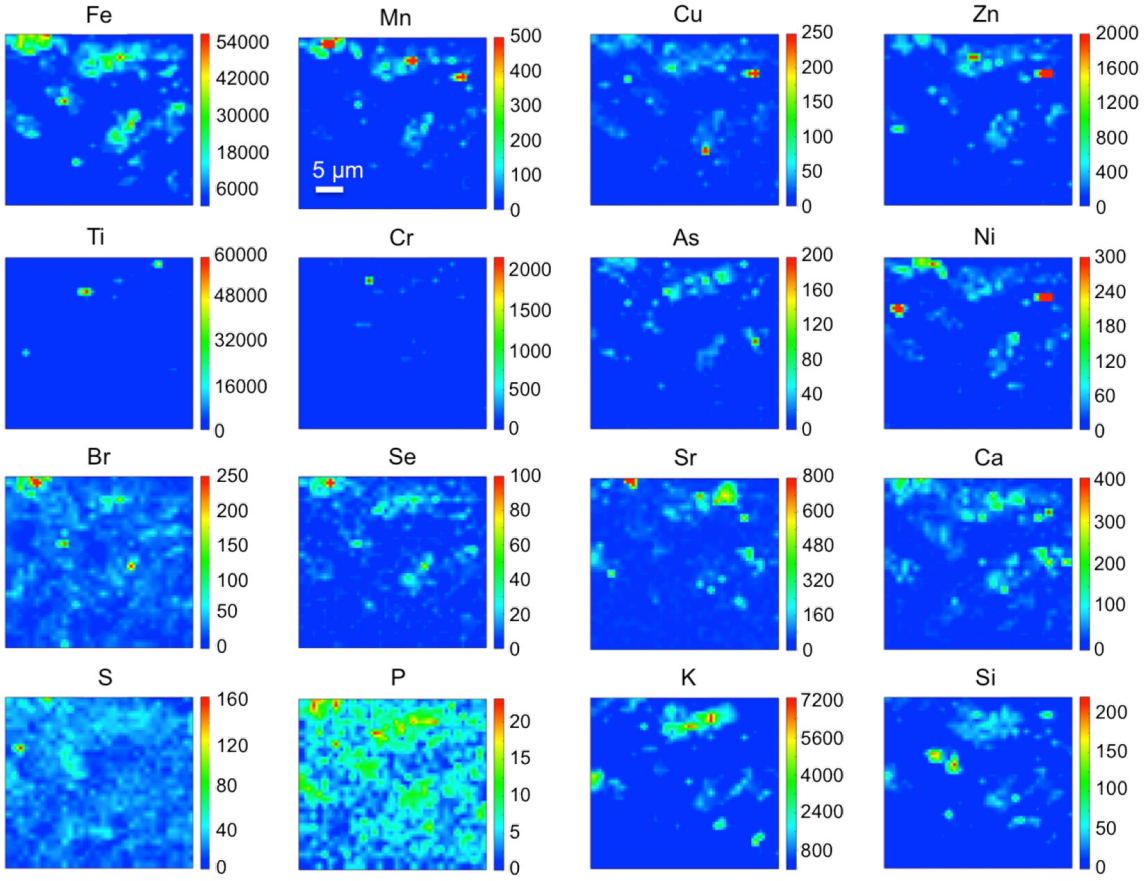

Fig. 2. XRF maps of Fe, Mn, Cu, Zn, Ti, Cr, As, Ni, Br, Se, Sr, Ca, S, P, K and Si acquired at ID16B-NA beamline (ESRF, Grenoble, France) in an anthracotic region with sub-micrometric spatial resolution. All XRF maps were acquired at 17 keV over an area of 34 µm × 34 µm with a spatial resolution of 0.5 µm and a dwell time of 100 ms/pixel in the raster scan. Color scale bars show the total counts for each chemical element.

[53], while Sr is frequently found associated to Ca [54]. It is clear that part of the Ca detected in the anthracotic formations is from endogenous origin.

Even if not easily detectable at this excitation energy, phosphor (P) and sulphur (S) are usually delineating the tissue matrix, with P more concentrated in cells' nucleus [36]. Like S and P, K is an endogenous element that is not well detected and resolved at this excitation energy. However the XRF maps show a relatively high potassium signal, indicating that there is a high concentration of this element in lung tissues, clearly linked to particulate exposure. Potassium appears to be associated with burning events [22], such as crop burning in rural areas [55]. Being a light element the same considerations on detectability apply for Si; despite the low Si signal measurable in air, it seems that K and Si have a similar distribution, partially co-localising in some areas, even though as expected, Si appears more spread in the tissue. Quite in agreement, a previous study showed that Si is the most abundant element in intrapulmonary particulate pollutants [56]. In order to better investigate Si and light elements distribution, low energy XRF measurements were carried out at 1.95 keV at TwinMic beamline (Elettra Sincrotrone Trieste, Trieste, Italy).

In order to avoid possible artifacts due to radiation damage [57] induced by the higher energy scans, the analysed areas were chosen in proximity, but not overlapping with the previous scanned ones or on consecutive slices. A rough estimate of the delivered dose on the sample shows indeed that with the ID16A set-up the specimen may receive up to 2.8×10^{12} Gy while with TwinMic one 7.7×10^{9} Gy. By using soft X-rays, high resolution absorption (Abs) and phase contrast (PhC) images where collected simultaneously, allowing to outline the morphological features of the lung tissue samples at sub-micrometer length scales. Fig. 4 shows the visible light image of one of the lung tissues analysed at TwinMic together with the corresponding absorption images. To note, dark areas in the absorption images indicate a denser, more absorbing material. The anthracotic regions, identified by black-pigmented areas visible in the optical images, appear as dark micro- and nano-agglomerates in the absorption images but with high contrast only in subregions of the pigmented areas. Surprisingly, their absorption signal and contrast is not much different from other less pigmented lung tissue areas. That means that without the comparison with visible light and histological images the anthracotic areas wouldn't be easily identified or distinguished in the absorption images. The major contributor of the anthracotic material seems to be a low density material, probably carbonaceous, while highly absorbing spots are related to metal and metalloid content. These observations only partially confirm what found in studies performed by other authors [58] where anthracotic granules appeared opaque in radiographies, similarly to calcifications. It seems in fact that anthracosis can be identified indirectly through lymph node and bronchial calcifications on CT scans [58]. These radiographic signals could be related to the concentrations of heavy elements (i.e Ni, Ti, Cr) and transition metals (Fe, Zn, Cu) together with high Si. However, the complete nature of anthracosis and its black-pigmented appearance is still elusive.

Fig. 5 shows two lung tissues regions analysed at TwinMic. Dark anthracotic areas are rich in Si and Al, which co-localise in many areas together with Fe, possibly identifying allumino-silicates, in agreement with previous studies [56]. In some agglomerates though, they seem to have a different distribution: indeed hot spots of Si delineating a nano-agglomerate do not always co-localise with hot spots of Al. The darkest features exhibit high Si signal, which appear as granules or in micrometric-long fibre form. It is well known that Al and Si are mostly present in PM as mineral matter, from crustal and road erosion [20] and

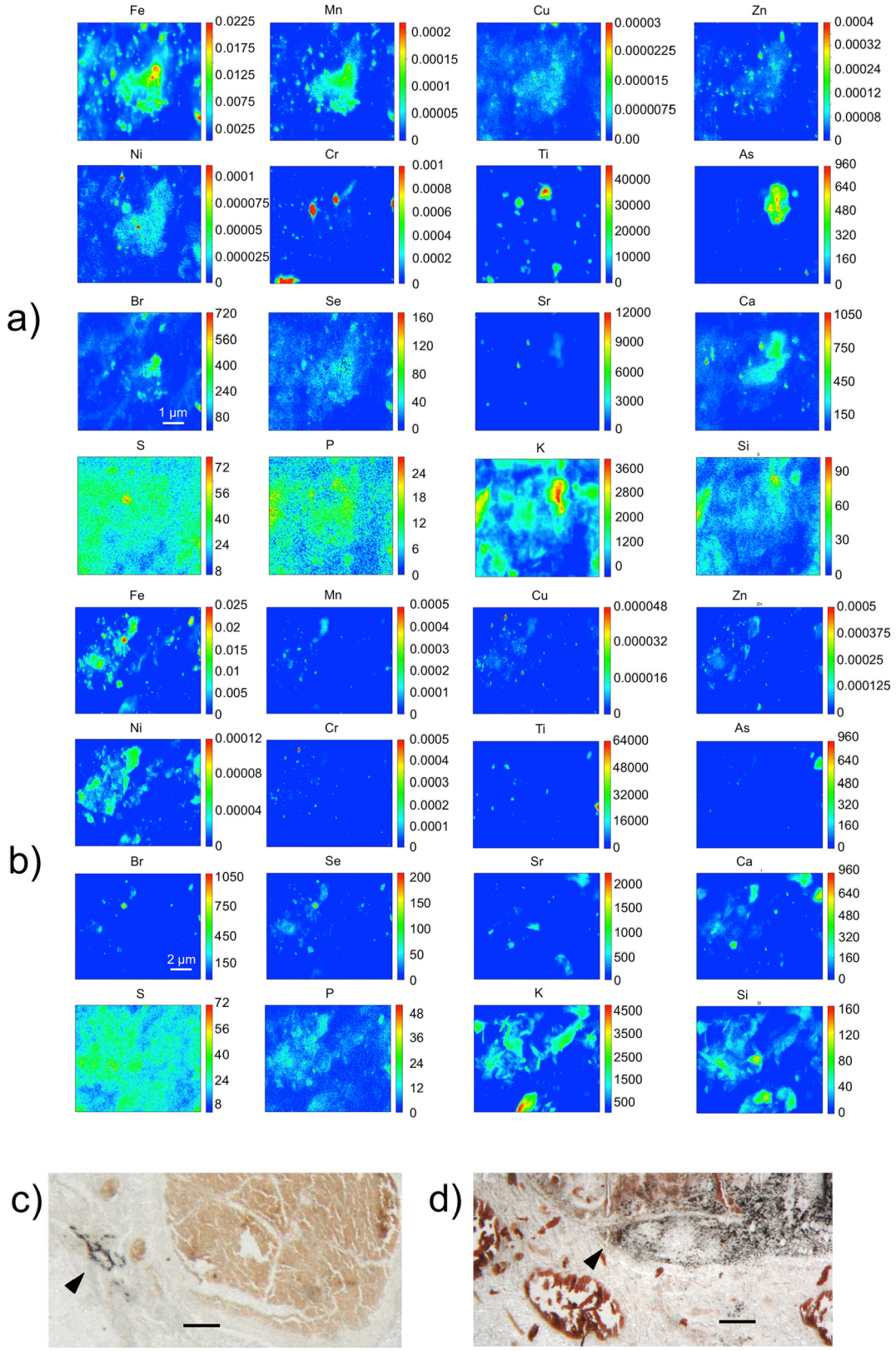

Fig. 3. XRF maps of Fe, Mn, Cu, Zn, Ti, Cr, As, Ni, Br, Se, Sr, Ca, S, P, K and Si acquired at ID16B-NA beamline (ESRF, Grenoble, France) in two anthracotic regions with nanometric spatial resolution. All XRF maps were acquired at 17.54 keV over an area of 6 µm × 6 µm (a) and 12 µm × 10 µm (b), with a spatial resolution of 50 nm and a dwell time of 100 ms/pixel in the raster scan. Color scale bars show the total counts for each chemical element, except for Cr, Mn, Fe, Ni, Cu and Zn where they are expressed in mass fraction (g/g). Panels c) and d) show visible light images of the lung tissue sections, indicating approximately the analysed areas depicted in a) and b) respectively. Scale bars are 100um for panels c) and d).

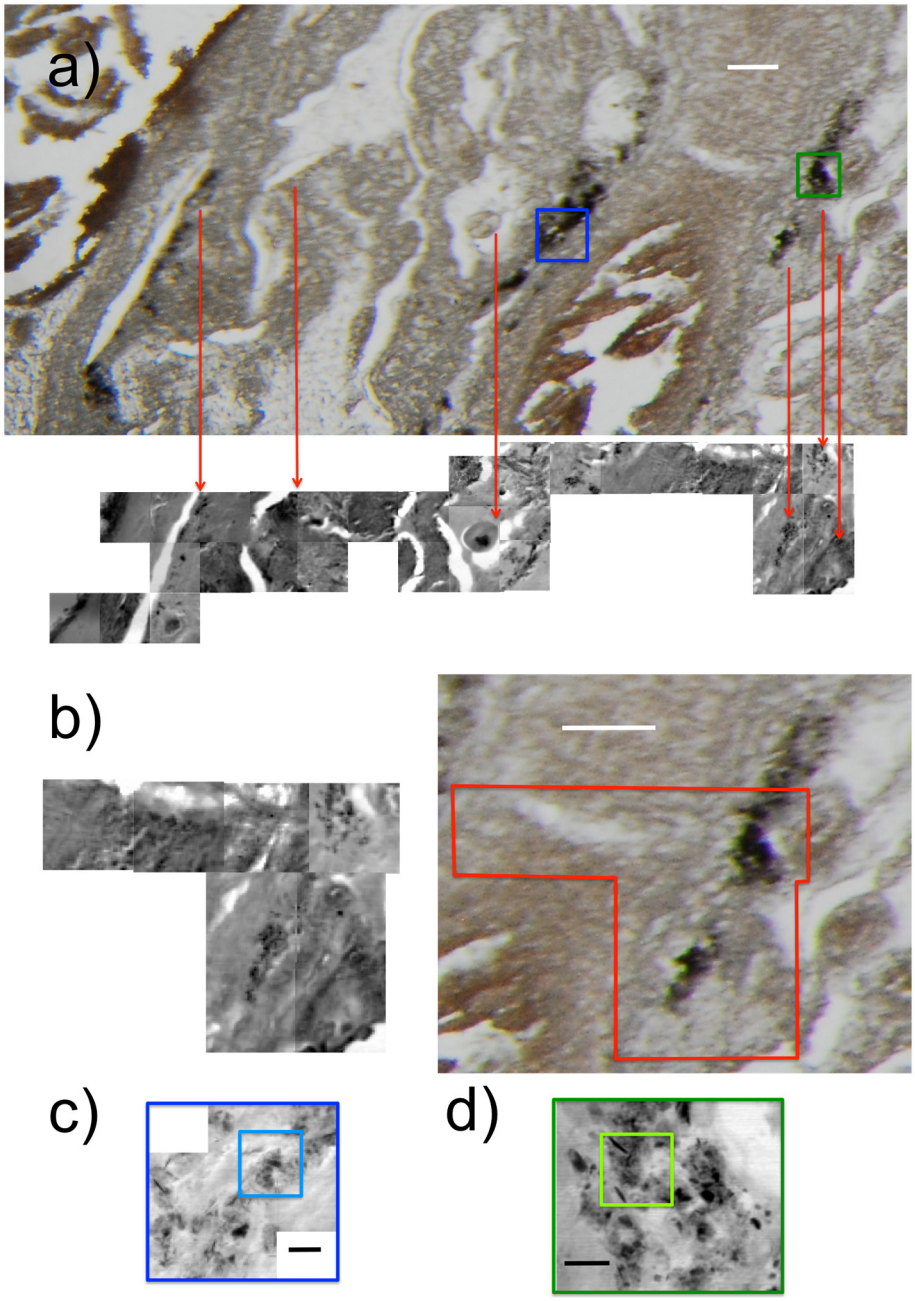

Fig. 4. Visible light (VL) image of one of the analysed lung tissues, depicted with the corresponding X-ray absorption image acquired at TwinMic beamline (Elettra Sincrotrone Trieste, Trieste, Italy). The anthracotic regions appear black-pigmented in the VL image. In panel (b) a zoom of an area of interest is shown, to better correlate absorption features (left panel) with VL ones (right panel). Scale bars are 80 µm for panels a) and b). Panels c) and d) depict absorption images of the areas delimited by the blue and green box in panel a). Scale bars are 10 µm for panels c) and d). The light blue box in panel c) and the light green box in panel d) show two areas mapped at TwinMic, shown in Fig. 5a and 5b respectively. (For interpretation of the references to color in this figure legend, the reader is referred to the web version of this article.)

therefore these two chemical elements are expected protagonists in anthracosis composition.

Magnesium often co-localises with Si and Al, but while Si and Al signals are quite diffused, Mg appears as nano-puntiform. Apart from a few exceptions, Na is more uniformly distributed in the tissue, similarly to S and P. Oxygen often co-localises with Si or Al, as well as with Fe, indicating the presence of their oxide forms.

Fig. S2 shows the elemental maps performed on a sub area of Fig. 5b at the ID16B-NA beamline, complementing the analyses done at TwinMic and once again confirming the complicate nature of anthracotic deposits. The observations made for Fig. 3 are applicable to Fig. S2.

On a final note, it is important to underline that chemical fixation is known to be a possible cause of alteration in the spatial and quantitative distributions of elements [59], especially diffusible elements, such as P, S and Ca [60]. Some other elements, such as Fe and Cu, are instead typically bound into proteins and will not easily leach from or be chelated out of a tissue [60]. Elemental rearrangement is definitely more pronounced in isolated cells, while should be less marked in tissues, which have a more complex architecture and structure. However redistribution in the nanoparticulate aggregates, which are the focus of the present research, is expected to be marginal since they appear as compact inclusions within the tissue.

4. Conclusions

In this study the chemical nature of the environmental dust found within lung tissue and its possible correlation with morphological appearance was investigated for the first time at the nanometric scale. In summary this study provides evidence that in tissue samples: i) XRF at nanometer resolution can identify multiple types of nanoparticulate and thus can help to reveal anthracosis origin; ii) XRF can quantify important elements in nanodeposits providing information on the presence of highly toxic materials (i.e. Cr); iii) high X-ray absorption does

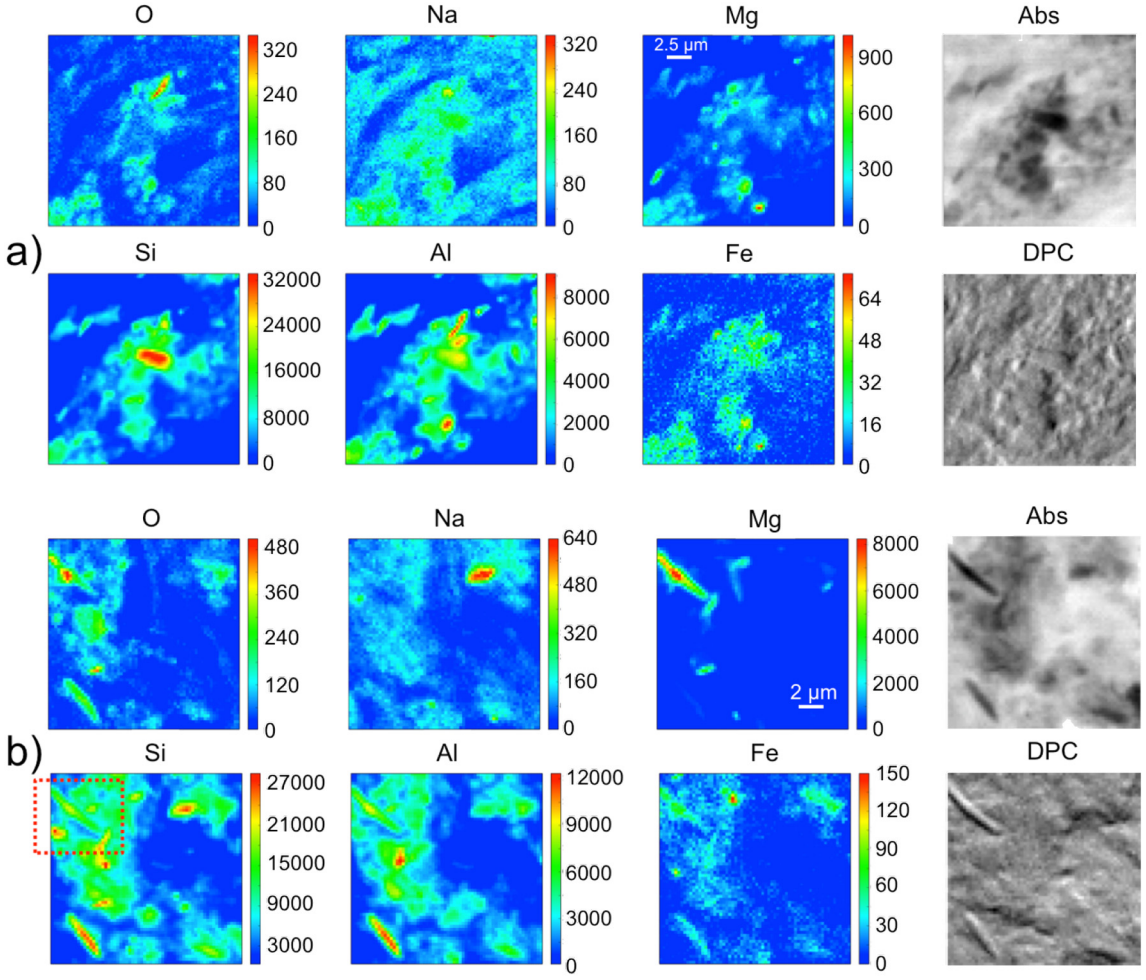

Fig. 5. Absorption (Abs) and differential phase contrast (DPC) images and corresponding XRF elemental maps of O, Na, Mg, Si, Al and Fe (acquired at TwinMic beamline at 1.95 keV with a spot size 250 nm in diameter and a dwell time of 9 s/pixel in the raster scan) over an area of 20 µm × 20 µm (a) and 16 µm × 16 µm (b). Color scale bars show the total counts for each chemical element. Red box indicates the area shown in Fig. S1. (For interpretation of the references to color in this figure legend, the reader is referred to the web version of this article.)

not necessarily correlate with black-pigmented deposits, whose color is most likely related to carbonaceous material; iv) low energy XRF allows to precisely identify Al and Si deposits correlating them with morphological features from absorption and phase contrast images.

Acknowledgment

The authors are grateful to Dr. G. Kourousias for helpful discussions and assistance in imaging processing and to Dr. M. W. M. Jones for assistance with the manuscript.

References

[1] C.J.L. Murray, A.D. Lopez, W.H. Organization, W. Bank, H.S. of P. Health, The Global burden of disease: a comprehensive assessment of mortality and disability from diseases, injuries, and risk factors in 1990 and projected to 2020: summary, http://www.who.int/iris/handle/10665/41864, (1996) , Accessed date: 12 February 2018.

[2] WHO|Global Health Estimates, http://www.who.int/healthinfo/global_burden_disease/en/, (2018) , Accessed date: 12 February 2018(n.d).

[3] M.P. Chung, K.S. Lee, J. Han, H. Kim, C.H. Rhee, Y.C. Han, O.J. Kwon, Bronchial stenosis due to anthracofibrosis, Chest 113 (1998) 344–350.

[4] O. Klotz, Pulmonary anthracosis — a community disease, Am. J. Public Health N. Y. N 1912 (4) (1914) 887–916.

[5] P.K. Sen, Pneumonoconiosis with special reference to silicosis, anthracosis and tuberculosis, Ind. Med. Gaz. 74 (1939) 547–554.

[6] L. Pascolo, V. Borelli, V. Canzonieri, A. Gianoncelli, G. Birarda, D.E. Bedolla, M. Salomé, L. Vaccari, C. Calligaro, M. Cotte, B. Hesse, F. Luisi, G. Zabucchi, M. Melato, C. Rizzardi, Differential protein folding and chemical changes in lung tissues exposed to asbestos or particulates, Sci. Rep. 5 (2015) 12129, http://dx.doi.org/10.1038/srep12129.

[7] J.M. Davis, J. Chapman, P. Collings, A.N. Douglas, J. Fernie, D. Lamb, V.A. Ruckley, Variations in the histological patterns of the lesions of coal workers' pneumoconiosis in Britain and their relationship to lung dust content, Am. Rev. Respir. Dis. 128 (1983) 118–124.

[8] J. Rosai, Surgical Pathology, Elsevier, 2011, p. 363.

[9] P. Lacy, Environmental pathobiology—the combined approach to problem solving and manpower training, Am. J. Pathol. 64 (1971) 217–224.

[10] Q. Zhang, X. Huang, Induction of ferritin and lipid peroxidation by coal samples with different prevalence of coal workers' pneumoconiosis: role of iron in the coals, Am. J. Ind. Med. 42 (2002) 171–179, http://dx.doi.org/10.1002/ajim.10101.

[11] D. Hayes, E. Diaz-Guzman, D.L. Davenport, J.B. Zwischenberger, M. Khosravi, K.J. Absher, C.W. Hoopes, Lung transplantation in patients with coal workers' pneumoconiosis, Clin. Transpl. 26 (2012) 629–634, http://dx.doi.org/10.1111/j.1399-0012.2011.01590.x.

[12] C. Huang, J. Li, Q. Zhang, X. Huang, Role of bioavailable iron in coal dust-induced activation of activator protein-1 and nuclear factor of activated T cells: difference between Pennsylvania and Utah coal dusts, Am. J. Respir. Cell Mol. Biol. 27 (2002) 568–574, http://dx.doi.org/10.1165/rcmb.4821.

[13] S. Ohshima, Studies on pulmonary anthracosis with special reference to the mineral constitution of intrapulmonary particulate pollutants in the human lung, Pathol. Int. 40 (1990) 41–49, http://dx.doi.org/10.1111/j.1440-1827.1990.tb01527.x.

[14] M. Mirsadraee, Anthracosis of the lungs: etiology, clinical manifestations and diagnosis: a review, Tanaffos. 13 (2014) 1–13.

[15] D. Loomis, Y. Grosse, B. Lauby-Secretan, F.E. Ghissassi, V. Bouvard, L. Benbrahim-

Tallaa, N. Guha, R. Baan, H. Mattock, K. Straif, The carcinogenicity of outdoor air pollution, Lancet Oncol. 14 (2013) 1262–1263, http://dx.doi.org/10.1016/S1470-2045(13)70487-X.
[16] L. Pascolo, A. Gianoncelli, C. Rizzardi, M. de Jonge, D. Howard, D. Paterson, F. Cammisuli, M. Salomé, P.D. Paoli, M. Melato, V. Canzonieri, Focused X-ray histological analyses to reveal asbestos fibers and bodies in lungs and pleura of asbestos-exposed subjects, Microsc. Microanal. 22 (2016) 1062–1071, http://dx.doi.org/10.1017/S1431927616011685.
[17] A.J. Buczyńska, A. Krata, R. Van Grieken, A. Brown, G. Polezer, K. De Wael, S. Potgieter-Vermaak, Composition of PM2.5 and PM1 on high and low pollution event days and its relation to indoor air quality in a home for the elderly, Sci. Total Environ. 490 (2014) 134–143, http://dx.doi.org/10.1016/j.scitotenv.2014.04.102.
[18] D. Cesari, A. Genga, P. Ielpo, M. Siciliano, G. Mascolo, F.M. Grasso, D. Contini, Source apportionment of $PM_{(2.5)}$ in the harbour-industrial area of Brindisi (Italy): identification and estimation of the contribution of in-port ship emissions, Sci. Total Environ. 497–498 (2014) 392–400, http://dx.doi.org/10.1016/j.scitotenv.2014.08.007.
[19] M. Khodeir, M. Shamy, M. Alghamdi, M. Zhong, H. Sun, M. Costa, L.-C. Chen, P. Maciejczyk, Source apportionment and elemental composition of $PM_{2.5}$ and PM_{10} in Jeddah City, Saudi Arabia, Atmos. Pollut. Res. 3 (2012) 331–340.
[20] A. Thorpe, R.M. Harrison, Sources and properties of non-exhaust particulate matter from road traffic: a review, Sci. Total Environ. 400 (2008) 270–282, http://dx.doi.org/10.1016/j.scitotenv.2008.06.007.
[21] J.J. Schauer, W.F. Rogge, L.M. Hildemann, M.A. Mazurek, G.R. Cass, B.R.T. Simoneit, Source apportionment of airborne particulate matter using organic compounds as tracers, Atmos. Environ. 30 (1996) 3837–3855, http://dx.doi.org/10.1016/1352-2310(96)00085-4.
[22] M. Viana, T.A.J. Kuhlbusch, X. Querol, A. Alastuey, R.M. Harrison, P.K. Hopke, W. Winiwarter, M. Vallius, S. Szidat, A.S.H. Prévôt, C. Hueglin, H. Bloemen, P. Wåhlin, R. Vecchi, A.I. Miranda, A. Kasper-Giebl, W. Maenhaut, R. Hitzenberger, Source apportionment of particulate matter in Europe: a review of methods and results, J. Aerosol Sci. 39 (2008) 827–849, http://dx.doi.org/10.1016/j.jaerosci.2008.05.007.
[23] J.-H. Tsai, L.T.-C. Chang, Y.-S. Huang, H.-L. Chiang, Particulate composition characteristics under different ambient air quality conditions, J. Air Waste Manage. Assoc. 1995 (61) (2011) 796–805.
[24] H.J. Annegarn, A.E. Pillay, J.C.A. Da Vies, D. Faure, J.P.F. Sellschop, PIXE analysis of mineral matter in thin sections of human lung, Nucl. Instrum. Methods Phys. Res., Sect. B 35 (1988) 415–419, http://dx.doi.org/10.1016/0168-583X(88)90303-5.
[25] Y. Shimizu, K. Dobashi, Proton ion-microbeam elemental analysis for inhaled particle-induced pulmonary diseases: application for diagnosis and assessment of progression, Curr. Med. Chem. 20 (2013) 789–793.
[26] Y. Shimizu, S. Matsuzaki, T. Satoh, M. Koka, A. Yokoyama, T. Ohkubo, Y. Ishii, T. Kamiya, M. Fueki, M. Mori, K. Dobashi, In-air microparticle induced X-ray emission analysis of particles in interstitial pneumonia lung tissue obtained by transbronchial biopsy, J. Clin. Biochem. Nutr. 49 (2011) 125–130, http://dx.doi.org/10.3164/jcbn.10-127.
[27] H. Chino, E. Hagiwara, M. Sugisaki, T. Baba, Y. Koga, T. Hisada, K. Kaira, K. Okudela, T. Takemura, K. Dobashi, T. Ogura, Pulmonary aluminosis diagnosed with in-air microparticle induced X-ray emission analysis of particles, Intern. Med. Tokyo Jpn. 54 (2015) 2035–2040, http://dx.doi.org/10.2169/internalmedicine.54.4246.
[28] X. He, H. Shen, Z. Chen, C. Rong, M. Ren, L. Hou, C. Wu, L. Mao, Q. Lu, B. Su, Element-based prognostics of occupational pneumoconiosis using micro-proton-induced X-ray emission analysis, Am. J. Phys. Lung Cell. Mol. Phys. (2017), http://dx.doi.org/10.1152/ajplung.00009.2017.
[29] E. Monsó, A. Carreres, J.M. Tura, J. Ruiz, J. Fiz, C. Xaus, M. Llatjós, J. Morera, Electron microscopic microanalysis of bronchoalveolar lavage: a way to identify exposure to silica and silicate dust, Occup. Environ. Med. 54 (1997) 560–565.
[30] K. Tsuchiya, N. Inase, S. Ichinose, Y. Usui, Y. Miyazaki, Y. Ohtani, N. Ando, T. Akashi, Y. Kondoh, H. Taniguchi, Y. Yoshizawa, Elemental analysis of inorganic dusts in lung tissues of interstitial pneumonias, J. Med. Dent. Sci. 54 (2007) 9–16.
[31] Applications of synchrotron radiation, Springer Berlin Heidelberg, Berlin, Heidelberg, http://link.springer.com/10.1007/978-3-540-46427-3, (2007) , Accessed date: 1 July 2016.
[32] J. Kirz, C. Jacobsen, M. Howells, Soft X-ray microscopes and their biological applications, Q. Rev. Biophys. 28 (1995) 33–130.
[33] B. Kaulich, P. Thibault, A. Gianoncelli, M. Kiskinova, Transmission and emission X-ray microscopy: operation modes, contrast mechanisms and applications, J. Phys. Condens. Matter Inst. Phys. J. 23 (2011) 083002, , http://dx.doi.org/10.1088/0953-8984/23/8/083002.
[34] L. Pascolo, F. Esteve, C. Rizzardi, S. James, R.H. Menk, Potential advantages of using synchrotron X-ray based techniques in pediatric research, Curr. Med. Chem. 20 (2013) 2157–2175.
[35] L. Pascolo, A. Gianoncelli, B. Kaulich, C. Rizzardi, M. Schneider, C. Bottin, M. Polentarutti, M. Kiskinova, A. Longoni, M. Melato, Synchrotron soft X-ray imaging and fluorescence microscopy reveal novel features of asbestos body morphology and composition in human lung tissues, Part. Fibre Toxicol. 8 (2011) 7, http://dx.doi.org/10.1186/1743-8977-8-7.
[36] L. Pascolo, A. Gianoncelli, G. Schneider, M. Salomé, M. Schneider, C. Calligaro, M. Kiskinova, M. Melato, C. Rizzardi, The interaction of asbestos and iron in lung tissue revealed by synchrotron-based scanning X-ray microscopy, Sci. Rep. 3 (2013), http://dx.doi.org/10.1038/srep01123.
[37] G. Martínez-Criado, J. Villanova, R. Tucoulou, D. Salomon, J.-P. Suuronen, S. Labouré, C. Guilloud, V. Valls, R. Barrett, E. Gagliardini, Y. Dabin, R. Baker, S. Bohic, C. Cohen, J. Morse, ID16B: a hard X-ray nanoprobe beamline at the ESRF for nano-analysis, J. Synchrotron Radiat. 23 (2016) 344–352, http://dx.doi.org/10.1107/S1600577515019839.
[38] A. Sole, E. Papillon, M. Cotte, P. Walter, J. Susini, A multiplatform code for the analysis of energy-dispersive X-ray fluorescence spectra, Spectrochim. Acta B At. Spectrosc. 62 (2007) 63–68, http://dx.doi.org/10.1016/j.sab.2006.12.002.
[39] A. Gianoncelli, G. Kourousias, L. Merolle, M. Altissimo, A. Bianco, Current status of the TwinMic beamline at Elettra: a soft X-ray transmission and emission microscopy station, J. Synchrotron Radiat. 23 (2016) 1526–1537, http://dx.doi.org/10.1107/S1600577516014405.
[40] A. Gianoncelli, G.R. Morrison, B. Kaulich, D. Bacescu, J. Kovac, Scanning transmission x-ray microscopy with a configurable detector, Appl. Phys. Lett. 89 (2006) 251117, http://dx.doi.org/10.1063/1.2422908.
[41] A. Gianoncelli, B. Kaulich, R. Alberti, T. Klatka, A. Longoni, A. De Marco, A. Marcello, M. Kiskinova, Simultaneous soft X-ray transmission and emission microscopy, Nucl. Instrum. Methods Phys. Res., Sect. A 608 (2009) 195–198, http://dx.doi.org/10.1016/j.nima.2009.06.035.
[42] A. Gianoncelli, G. Kourousias, A. Stolfa, B. Kaulich, Recent developments at the TwinMic beamline at ELETTRA: an 8 SDD detector setup for low energy X-ray fluorescence, J. Phys. Conf. Ser. 425 (2013) 182001, http://dx.doi.org/10.1088/1742-6596/425/18/182001.
[43] K.A. Prather, C.D. Hatch, V.H. Grassian, Analysis of atmospheric aerosols, Annu. Rev. Anal. Chem. 1 (2008) 485–514, http://dx.doi.org/10.1146/annurev.anchem.1.031207.113030.
[44] R.J. Charlson, S.E. Schwartz, J.M. Hales, R.D. Cess, J.A. Coakley, J.E. Hansen, D.J. Hofmann, Climate forcing by anthropogenic aerosols, Science 255 (1992) 423–430, http://dx.doi.org/10.1126/science.255.5043.423.
[45] M.L. López, S. Ceppi, G.G. Palancar, L.E. Olcese, G. Tirao, B.M. Toselli, Elemental concentration and source identification of PM_{10} and $PM_{2.5}$ by SR-XRF in Córdoba City, Argentina, Atmos. Environ. 45 (2011) 5450–5457, http://dx.doi.org/10.1016/j.atmosenv.2011.07.003.
[46] N.A. Janssen, G. Hoek, B. Brunekreef, H. Harssema, Mass concentration and elemental composition of PM_{10} in classrooms, Occup. Environ. Med. 56 (1999) 482–487.
[47] D. Cesari, A. Donateo, M. Conte, D. Contini, Inter-comparison of source apportionment of PM10 using PMF and CMB in three sites nearby an industrial area in Central Italy, Atmos. Res. 182 (2016) 282–293, http://dx.doi.org/10.1016/j.atmosres.2016.08.003.
[48] R. Gabriel, R. von Glasow, R. Sander, M.O. Andreae, P.J. Crutzen, Bromide content of sea-salt aerosol particles collected over the Indian Ocean during INDOEX 1999, J. Geophys. Res. Atmos. 107 (2002) (INX2 31-1), https://doi.org/10.1029/2001JD001133.
[49] M.S. Germani, M. Small, W.H. Zoller, J.L. Moyers, Fractionation of elements during copper smelting, Environ. Sci. Technol. 15 (1981) 299–305, http://dx.doi.org/10.1021/es00085a005.
[50] J. Vehlow, B. Bergfeldt, H. Hunsinger, H. Seifert, F.E. Mark, Bromine in waste incineration: partitioning and influence on metal volatilisation, Environ. Sci. Pollut. Res. Int. 10 (2003) 329–334.
[51] R.O. Gonzalez, S. Strekopytov, F. Amato, X. Querol, C. Reche, D. Weiss, New insights from zinc and copper isotopic compositions into the sources of atmospheric particulate matter from two major European cities, Environ. Sci. Technol. 50 (2016) 9816–9824, http://dx.doi.org/10.1021/acs.est.6b00863.
[52] D.J. Eide, The oxidative stress of zinc deficiency, Metallomics 3 (2011) 1124–1129, http://dx.doi.org/10.1039/C1MT00064K.
[53] J.-Y. Chung, S.-D. Yu, Y.-S. Hong, Environmental source of arsenic exposure, J. Prev. Med. Public Health 47 (2014) 253–257, http://dx.doi.org/10.3961/jpmph.14.036.
[54] I. Rivas, M. Viana, T. Moreno, M. Pandolfi, F. Amato, C. Reche, L. Bouso, M. Àlvarez-Pedrerol, A. Alastuey, J. Sunyer, X. Querol, Child exposure to indoor and outdoor air pollutants in schools in Barcelona, Spain, Environ. Int. 69 (2014) 200–212, http://dx.doi.org/10.1016/j.envint.2014.04.009.
[55] N. Singh, S.K. Mittal, R. Singh, R. Agarwal, A. Awasthi, P.K. Gupta, Potassium as a marker in air particulate matter after crop residue burning events in Patiala, India, Chitkara Chem. Rev. 1 (2013) 47–58, http://dx.doi.org/10.15415/ccr.2013.12010.
[56] S. Ohshima, Studies on pulmonary anthracosis. With special reference to the mineral constitution of intrapulmonary particulate pollutants in the human lung, Acta Pathol. Jpn. 40 (1990) 41–49.
[57] D.E. Bedolla, A. Mantuano, A. Pickler, C.L. Mota, D. Braz, C. Salata, C.E. Almeida, G. Birarda, L. Vaccari, R.C. Barroso, A. Gianoncelli, Effects of soft X-ray radiation damage on paraffin-embedded rat tissues supported on ultralene: a chemical perspective, J. Synchrotron Radiat. 25 (2018), http://dx.doi.org/10.1107/S1600577518003235.
[58] M. Mirsadraee, A. Asna-Ashari, D. Attaran, S. Naghibi, S. Mirsadraee, Bronchial anthracosis: a new diagnosis for benign mass lesions of the lung, Tanaffos. 12 (2013) 10–18.
[59] L. Perrin, A. Carmona, S. Roudeau, R. Ortega, Evaluation of sample preparation methods for single cell quantitative elemental imaging using proton or synchrotron radiation focused beams, J. Anal. At. Spectrom. 30 (2015) 2525–2532, http://dx.doi.org/10.1039/C5JA00303B.
[60] S.A. James, D.E. Myers, M.D. de Jonge, S. Vogt, C.G. Ryan, B.A. Sexton, P. Hoobin, D. Paterson, D.L. Howard, S.C. Mayo, M. Altissimo, G.F. Moorhead, S.W. Wilkins, Quantitative comparison of preparation methodologies for X-ray fluorescence microscopy of brain tissue, Anal. Bioanal. Chem. 401 (2011) 853–864, http://dx.doi.org/10.1007/s00216-011-4978-3.